Supplementary Information

Diesel soot-derived high-performance anode material for Lithium/Sodium-ion Batteries: impact of different annealing temperature

LIU Heng-rui[1], BAI Qing-yang[1], MA Chao[2,*]

1. School of Mechanical Engineering, Shanghai Jiao Tong University, Shanghai, 200240, P.R. China.

2. College of Smart Energy, Shanghai Jiao Tong University, Shanghai, 200240, P.R. China.

Corresponding author: MA Chao, chaoma99@sjtu.edu.cn

Table S1. Diesel engine specifications.

Parameter	Value
Maximum Power	55 kW
Maximum Speed	2400 rpm
Manufacturing Date	September 2018
Compliance Standard	GB/T1147.1

Table S2. Results from XRD, Raman and BET tests.

Material	d002 (Å)	ID/IG	BET Specific Surface Area (m^2/g)	Total Pore Volume (cm^3/g)	Average Pore Diameter (nm)	Micropore Volume (cm^3/g)
S-800	3.55	0.98	163.6	0.198	12.9	0.048
S-900	3.52	0.96	134.0	0.205	13.7	0.033
S-1000	3.50	0.92	91.4	0.211	15.1	0.014

Table S3. Concentrations of impurity elements in the soot materials.

Material	Fe (wt%)	Ca (wt%)	Zn (wt%)	S (wt%)	Si (wt%)
S-raw	1.501	0.784	0.032	0.047	0.033
Pr-S-800	1.313	0.845	0.048	0.048	0.026
Pr-S-900	1.415	1.044	0.040	0.021	0.046
Pr-S-1000	1.518	0.958	0.038	0.030	0.009
S-800	0.086	0.073	0.034	0.046	0.014
S-900	0.069	0.077	0.024	0.043	0.016
S-1000	0.054	0.084	0.011	0.024	0.040

Table S4. Reversible specific capacity at different current densities of S-raw, Pr-S-800, Pr-S-900, Pr-S-1000, S-800, S-900 and S-1000.

Material	Specific Capacity under Different C-rate (mAh/g)						
	C-rate						
	0.05 A/g	0.1 A/g (8^{th} cycle)	0.2 A/g	0.5 A/g	1 A/g	2 A/g	0.1 A/g (35^{th} cycle)
S-raw	382	224	127	74	46	28	142
Pr-S-800	377	329	280	176	133	92	301
Pr-S-900	606	537	455	411	266	194	498
Pr-S-1000	452	410	329	258	200	147	378
S-800	386	336	309	264	230	198	348
S-900	613	547	493	502	372	318	522
S-1000	462	418	384	352	319	282	412

Table S5. EIS fitting data for S-800, S-900 and S-1000.

Material	Cycle Number	R_s (ohm)	R_{SEI} (ohm)	R_{ct} (ohm)
S-800	0	2.2	0	81.0
	10	2.6	6.3	51.6
	50	3.4	7.9	33.2
	100	4.0	8.1	53.3
S-900	0	2.1	0	45.7
	10	2.9	3.0	36.5
	50	3.9	6.2	30.2
	100	7.6	8.4	24.3
S-1000	0	3.9	0	75.3
	10	4.1	1.7	51.7
	50	4.9	8.8	35.5
	100	4.0	9.1	27.2

Table S6. Charge capacity of various carbon-based electrode materials reported.

No.	Carbon Source	Charge Capacity (mAh/g)	Rate	Reference
1	Mangrove-charcoal	524	0.03 A/g	1
2	Rice straw	547	0.5 C	2
3	Cherry stones	348	0.2 C	3
4	Olive stones	170	0.2 C	4
5	Cotton wool	560	50 μA/cm^2	5
6	Rice husk	234	0.1 C	6
7	Human Hair	610	0.1 A/g	7
8	Naval ship marine gas oil soot	544	0.1 C	8
9	Electrostatic collected diesel soot	154	0.1 C	9
10	Candle soot	831	0.15 A/g	10
11	Lotus root	725	0.1 A/g	11
12	Merchant ship heavy oil soot	254	0.2 C	12
13	Diesel soot	109	0.1 C	13
14	Light diesel oil soot	626	0.1 A/g	Our Work

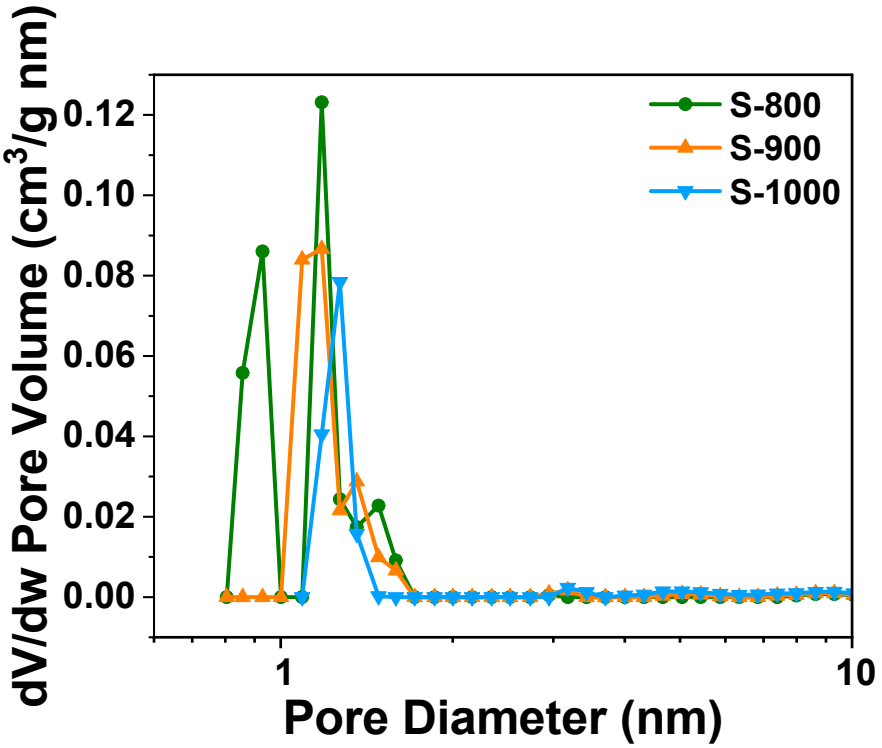

Figure S1. Micropore size distribution calculated from adsorption isotherms using the NLDFT of S-800, S-900 and S-1000.

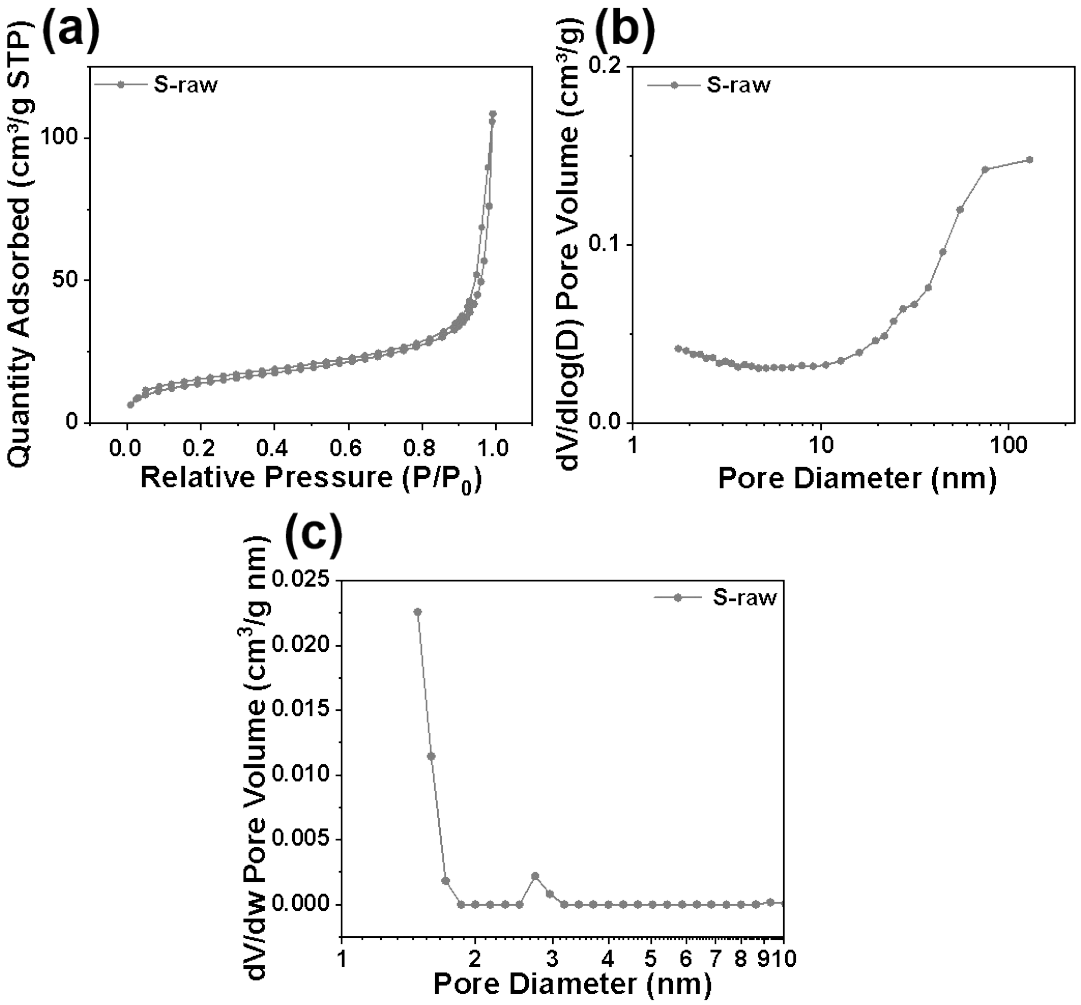

Figure S2. (a) Nitrogen adsorption and desorption isotherm, (b) BJH pore size distribution and (c) micropore size distribution calculated from adsorption isotherms using the NLDFT of S-raw.

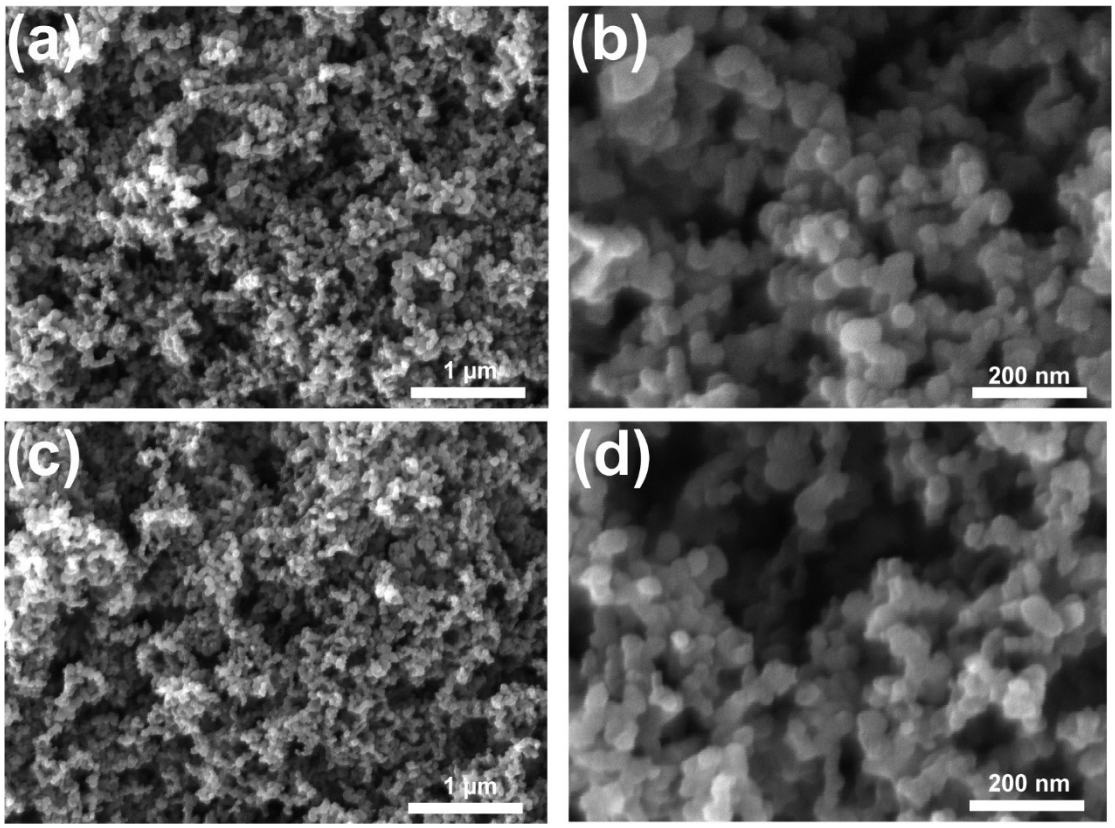

Figure S3. SEM micrographs of (a,b) S-800 and (c,d) S-1000.

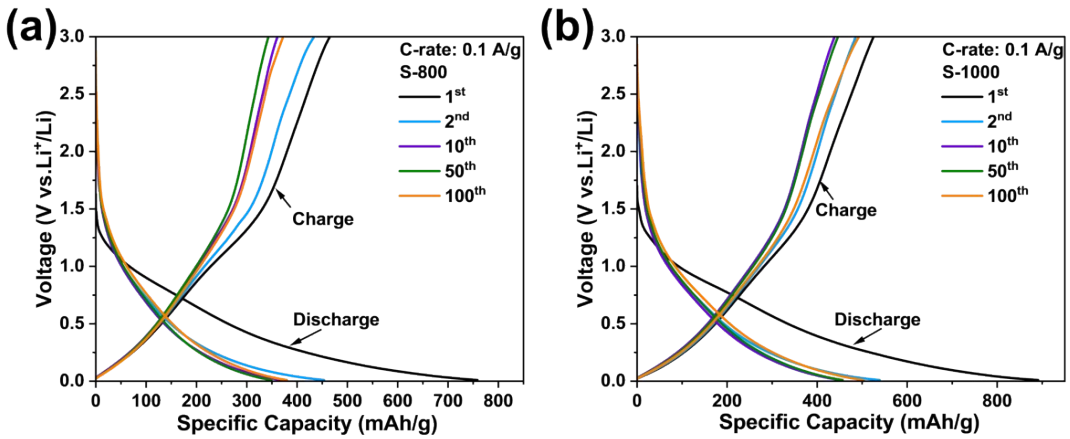

Figure S4. Charge/discharge profiles of the first, second, tenth, fiftieth, and hundredth cycles of (a) S-900 and (b) S-1000.

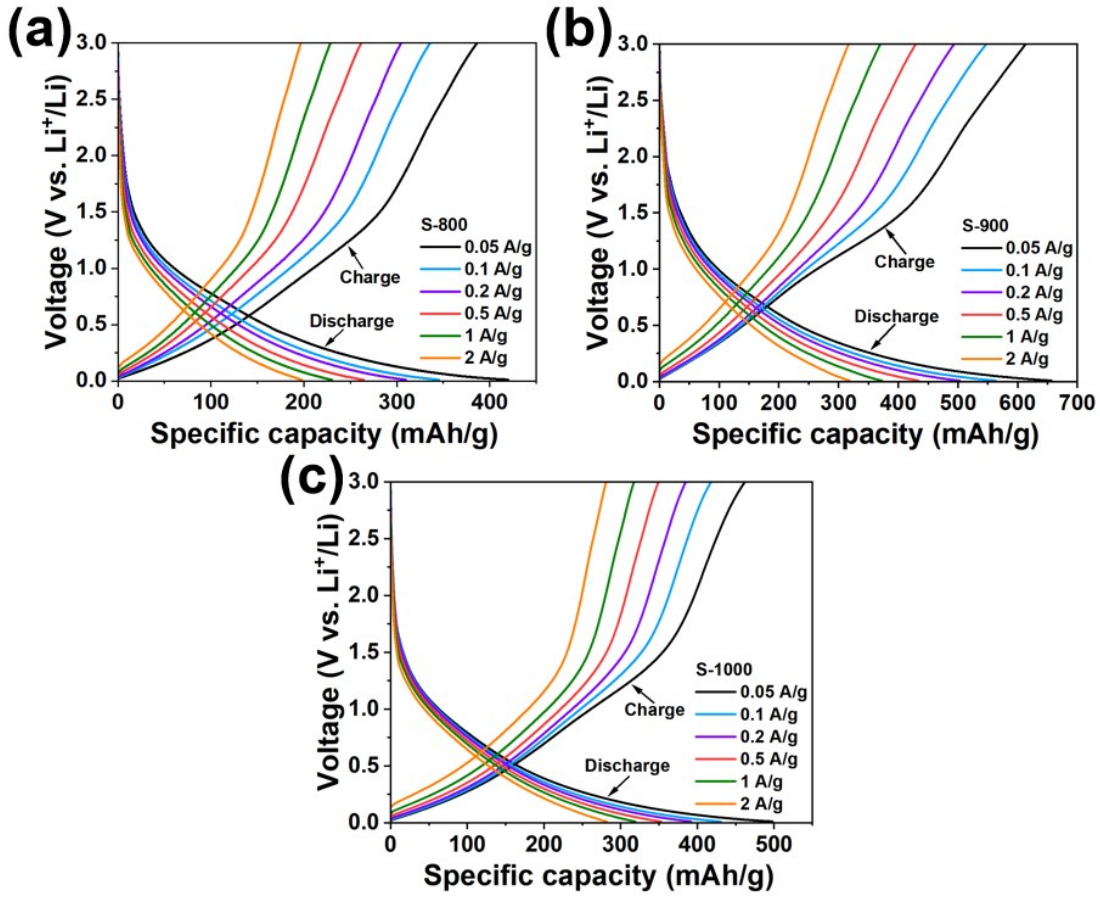

Figure S5. Charge/discharge profiles at 0.05, 0.1, 0.2, 0.5, 1 and 2 A/g of (a) S-800, (b) S-900 and (c) S-1000.

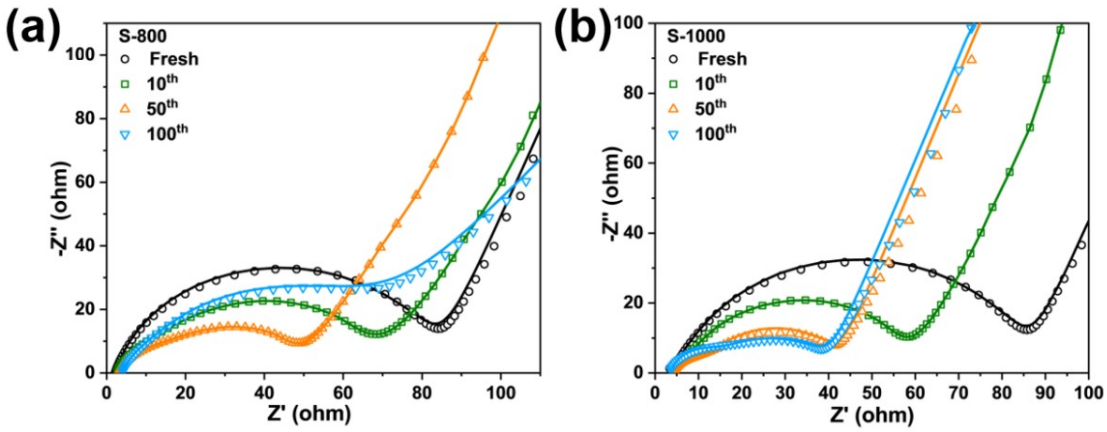

Figure S6. Nyquist plots before cycle and after tenth, fiftieth, and hundredth cycles at 1 A/g of (a) S-900 and (b) S-1000.

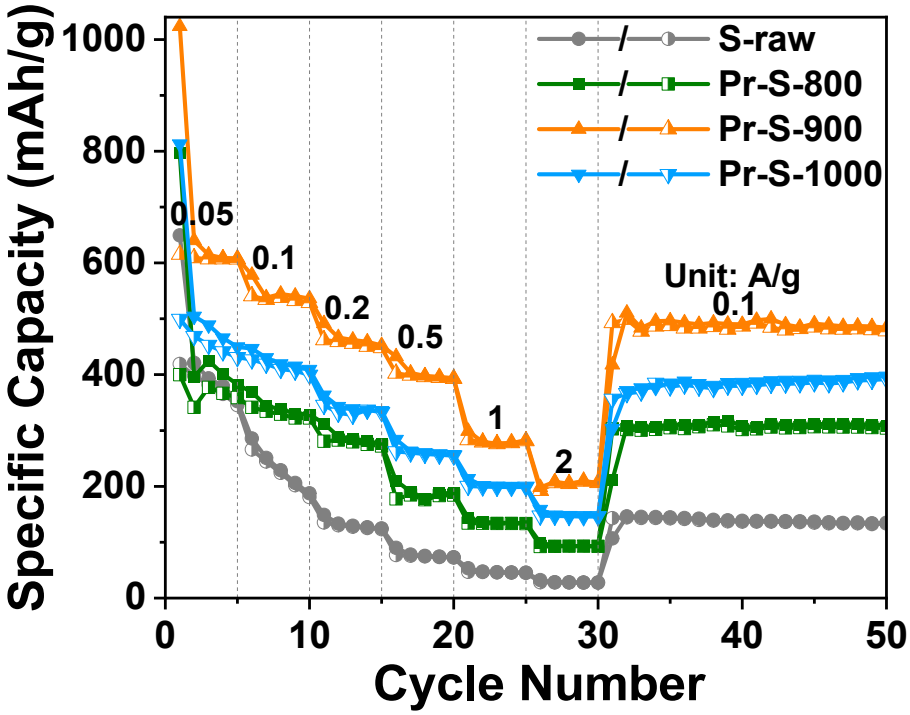

Figure S7. Rate performance of S-raw, Pr-S-800, Pr-S-900 and Pr-S-1000.

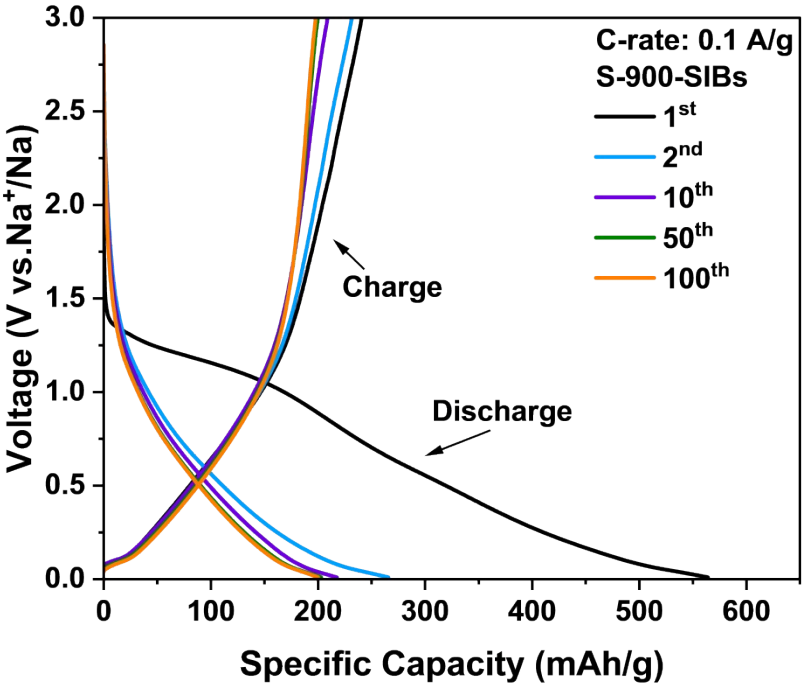

Figure S8. Charge/discharge profiles of the first, second, tenth, fiftieth, and hundredth cycles of S-900-SIBs.

Notes and references

1 T. Liu, R. Luo, W. Qiao, S.-H. Yoon and I. Mochida, *Electrochim. Acta*, 2010, **55**, 1696–1700.

2 F. Zhang, K.-X. Wang, G.-D. Li and J.-S. Chen, *Electrochem. Commun.*, 2009, **11**, 130–133.

3 J. C. Arrebola, A. Caballero, L. Hernán, J. Morales, M. Olivares-Marín and V. Gómez-Serrano, *J. Electrochem. Soc.*, 2010, **157**, A791.

4 A. Caballero, L. Hernán and J. Morales, *ChemSusChem*, 2011, **4**, 658–663.

5 E. Peled, V. Eshkenazi and Y. Rosenberg, *J. Power Sources*, 1998, **76**, 153–158.

6 G. T.-K. Fey and C.-L. Chen, *J. Power Sources*, 2001, **97–98**, 47–51.

7 Kr. Saravanan and N. Kalaiselvi, *Carbon*, 2015, **81**, 43–53.

8 H.-M. Baek, D.-Y. Kim, W.-J. Lee and J. Kang, *RSC Adv.*, 2020, **10**, 36478–36484.

9 D. Gregory, S. Yang, C. Massion, M. Mecklenburg, I. Aravind, M. Radonjic, S. Cronin and Ö. Ö. Çapraz, *Resour. Conserv. Recycl.*, 2022, **177**, 105972.

10 R. Kanakaraj and C. Sudakar, *J. Power Sources*, 2020, **458**, 228064.

11 H. Li, H. Luo, J. Teng, S. Yuan, J. Li, Y. Zhang, H. Duan and J. Li, *Chem. Select*, 2022, **7**, e202202413.

12 W.-J. Lee, H. V. Kim, J.-H. Choi, G. Panomsuwan, Y.-C. Lee, B.-S. Rho and J. Kang, *Sci. Rep.*, 2018, **8**, 5601.

13 S. Yang, B. Ozdogru, C. Ketelsleger, D. Gregory, Ö. Ö. Çapraz and S. B. Cronin, *Resour. Conserv. Recycl.*, 2021, **169**, 105485.